



2

Normative Measurements of Orbital Walls and Contents

Mathew B. Macey, Juan E. Small,
and Daniel Thomas Ginat

2.1 Orbital Walls

Each orbit is surrounded by medial, superior, lateral, and inferior orbital walls, which have a pyramidal configuration with the apex posteriorly. Several anatomical landmarks can be used to ascertain the separation between the two orbits (Fig. 2.1).

Interorbital distance (measured at the posterior border of the frontal processes of the maxilla in the plane of the optic nerve):

- At birth: 14.2 ± 0.7 mm
- At 1 year: 16.2 ± 0.8 mm

M. B. Macey
New York Institute of Technology College of Osteopathic Medicine,
Old Westbury, NY, USA

J. E. Small
Department of Radiology, Section of Neuroradiology,
Lahey Hospital and Medical Center, Burlington, MA, USA

D. T. Ginat (✉)
Department of Radiology, Section of Neuroradiology,
University of Chicago, Chicago, IL, USA
e-mail: dtg1@uchicago.edu

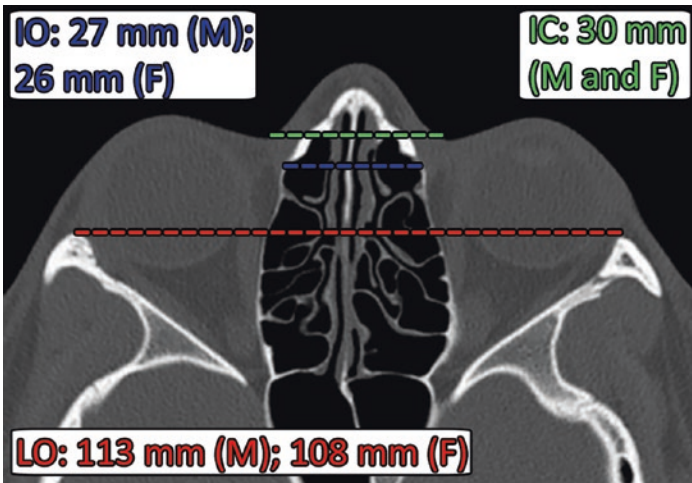


Fig. 2.1 Interorbital (IO), intercanthal (IC), and lateral orbital (LO) distances. Axial computed tomography (CT) image shows the typical measurements for adult males (M) and females (F)

- Adult males: 27 mm (range: 23–32 mm)
- Adult females: 26 mm (range: 23–32 mm)

The normal interorbital distance measured at the posterior border of the frontal processes of the maxilla on nonrotated scans, in the plane of the optic nerve, ranges from 23 to 32 mm (average: 27 mm) in men and 23 to 32 mm (average: 26 mm) in women. The widest interorbital (IO) distance lies behind the posterior poles of the globes. This ranges from 32 to 41 mm (average: 34 mm) in men and 29 to 37 mm (average: 32 mm) in women.

Inner intercanthal (IC) distance (measured between the medial canthi):

- At birth: 22 ± 1 mm
- At 1 year: 28 ± 1 mm
- Adult male: 30 mm (range: 27–35 mm)
- Adult female: 30 mm (range: 25–33 mm)

Lateral orbital (LO) distance (measured between the lateral orbital rims):

- Average at birth: 66 ± 2 mm
- Average at 1 year: 78 ± 2 mm
- Adult male average: 113 mm (range: 105–120 mm)
- Adult female average: 108 mm (range: 98–115 mm)

Practical implications: Normal measurements of orbital relationships are a useful reference for evaluating hypo- and hyper-telorism associated with craniofacial abnormalities and surgical reconstruction. Measurements are most reliable based on images in the Frankfort horizontal plane, which joins the anthropometric landmarks of porion and orbitale (Fig. 2.2).

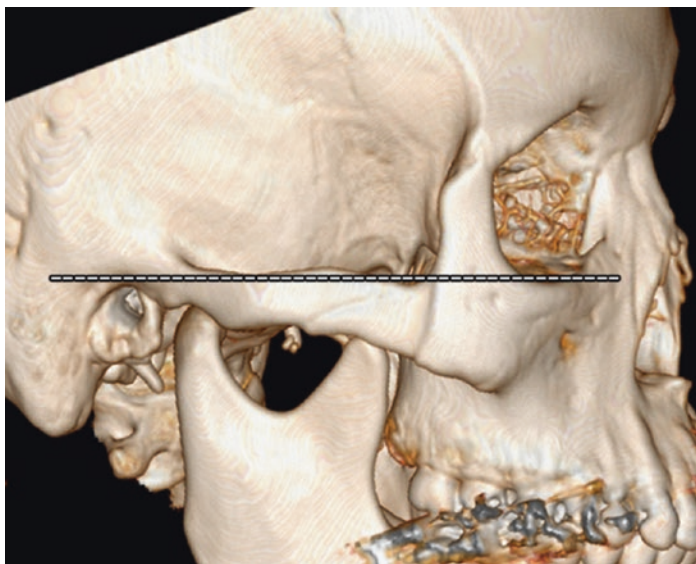


Fig. 2.2 Frankfort horizontal plane. Lateral 3D computed tomography (CT) image shows the orientation of the Frankfort horizontal plane, which extends from the superior aspect of the external auditory canal to the inferior orbital rim

Lateral Wall:

- The lateral orbital wall is formed by the greater wing of the sphenoid, frontal, and zygomatic bones.
- The deep lateral orbital wall comprises the sphenoid trigone, which has a triangular configuration on axial images.
- The typical distance of the lateral orbital rim to the apex is 35–40 mm in adults (Fig. 2.3).
- The average distance from the lateral orbital rim to the point where the lateral rectus muscle contacted the bone is 25–26 mm.



Fig. 2.3 Lateral orbital wall. Axial computed tomography (CT) image shows the average distance from the lateral orbital rim to the orbital apex

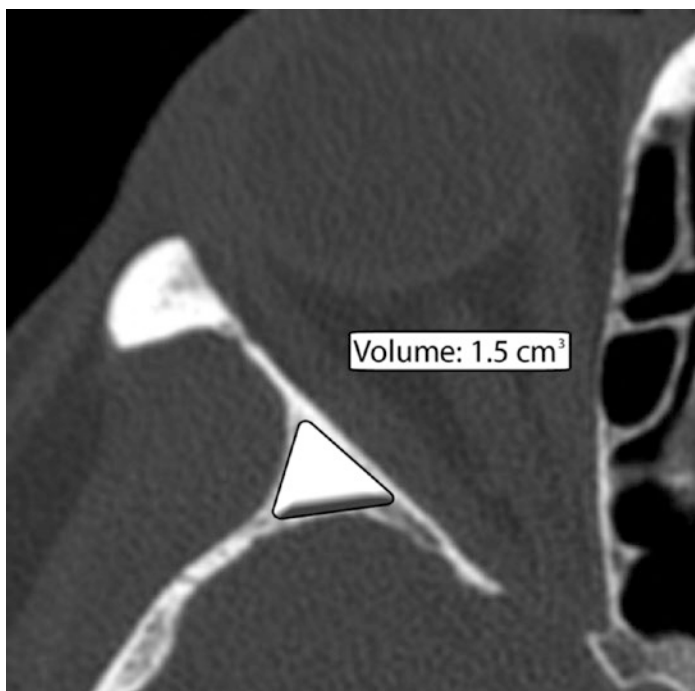


Fig. 2.4 Sphenoid trigone. Axial computed tomography (CT) image shows the overall sphenoid trigone volume

- The average width of the lateral wall at the level of the superior border of the lateral rectus muscle at the thickest part on the coronal image is 16 mm.
- The sphenoid trigone has an average volume of 1.5 cm³ (Fig. 2.4).

Practical implications: The deep lateral orbital wall is considered an effective and safe site for orbital decompression surgery. The degree of lateral decompression is dependent on the volume of the sphenoid trigone comprising the deep lateral orbital wall. The width and length of the thickest segment of the greater wing of the sphenoid can be used as anatomic guidelines during deep lateral orbital decompression surgery.

Medial Wall:

- The distance of the medial orbital rim to the apex is approximately 45 mm.
- The anterior ethmoid foramen, which contains the anterior ethmoidal artery, is located approximately 15 mm posterior to the medial orbital rim at the level of the junction of the frontal bone with the ethmoid bone (Fig. 2.5).
- Approximately 12 mm more posteriorly is the posterior ethmoid foramen through which the posterior ethmoidal artery passes.

Practical implications: The ethmoid arteries can be the source of epistaxis and orbital hemorrhage. Therefore, it is important to have a sense of where these are located for surgery in the medial orbital wall region.

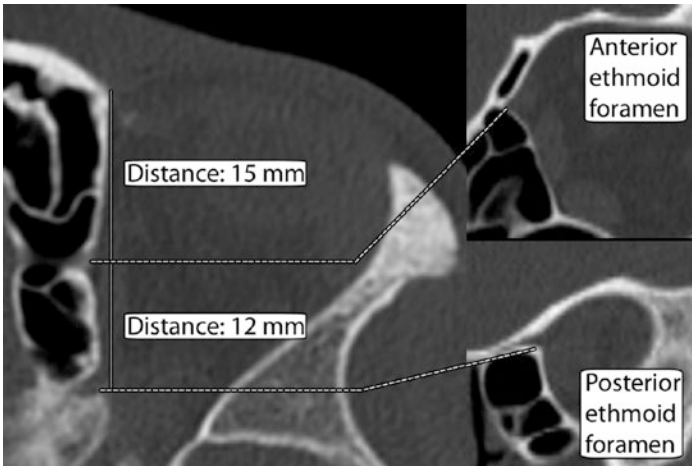


Fig. 2.5 Medial orbital wall. Axial and coronal computed tomography (CT) images depict the typical location of the anterior and posterior ethmoid foramina along the medial orbital wall

Inferior Orbital (Sphenomaxillary) Fissure:

- The inferior orbital fissure is located in the orbital floor adjacent to the superior orbital fissure, foramen rotundum, pterygopalatine fossa, infratemporal fossa, and temporal fossa.
- Bounded by the lower margin of the orbital surface of the greater wing of the sphenoid, laterally by the zygoma, posteromedially by the orbital process of the palatine bone, and anteriorly by the maxilla.
- Transmits the infraorbital nerve and artery.
- Oriented in an anterolateral direction from the maxillary strut posteriorly to the zygomatic bone anteriorly.
- Narrower at its center and its long axis lies along the line between the zygomaticofacial foramen and the optic canal.
- The average length of the inferior orbital fissure is 29 mm, with a range of 25–35 mm (Fig. 2.6).

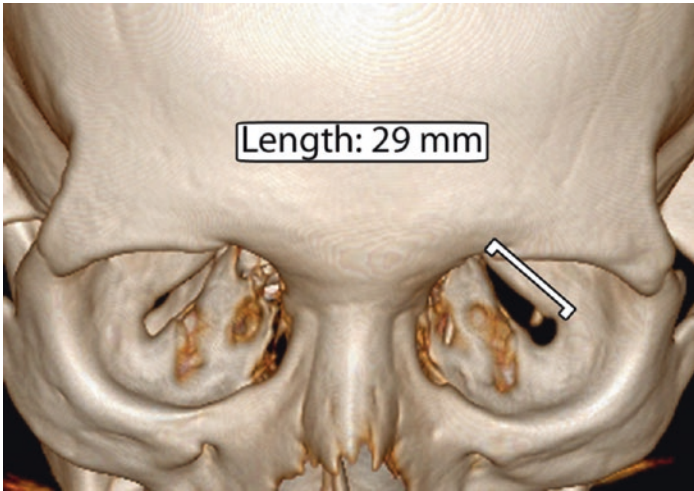


Fig. 2.6 Inferior orbital fissure. 3D computed tomography (CT) image shows the typical length of the inferior orbital fissure

Practical implications: The inferior orbital fissure is an important anatomic landmark for endonasal endoscopic approaches to the skull base and orbit.

Infraorbital Nerve Canal:

- The infraorbital nerve canal transmits the infraorbital nerve, which is the termination of the maxillary nerve and provides sensory function.
- The nerve exits the skull through the foramen rotundum and enters into the pterygopalatine fossa. It then enters the infraorbital groove and passes through the infraorbital canal. The nerve emerges in front of the maxilla through the infraorbital foramen.
- The mean infraorbital foramen to infraorbital margin distance is 7 ± 1 mm (Fig. 2.7).

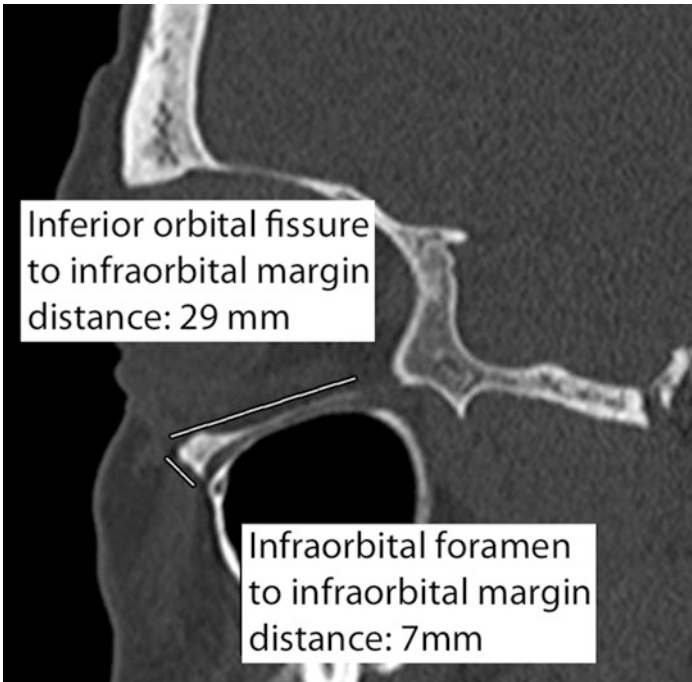


Fig. 2.7 Infraorbital canal. Sagittal computed tomography (CT) image shows the relation of the infraorbital nerve to neighboring landmarks

- The distance from the inferior orbital fissure to the infraorbital margin is 29 ± 2 mm.

Practical implications: The infraorbital nerve is at risk for iatrogenic injury during orbital floor repair.

2.2 Globe

- The globe occupies one-third of the overall orbital volume and consists of the outer wall, anterior chamber, lens, and vitreous body.
- The wall of the globe comprises three layers: the outer fibrous coat (sclera and cornea), the uvea (iris, ciliary body, and choroid), and the retina.
- The full-term newborn globe mean axial length is 16–18 mm.
- The globe (axial length) tends to grow until 16–18 years of age. Axial length, anterior chamber depth, and vitreous chamber depth then decrease with age, while lens thickness increases with age.
- Growth of the globe stops within 1 year after birth, with a mean globe diameter of 23 mm (range: 22–25 mm) (Fig. 2.8).
- The normal position of the posterior margin of the globe on axial CT images is 9–10 mm posterior to the interzygomatic line on average (range: 6–13 mm).
- The sclera measures up to 1 mm in thickness and appears hypointense on magnetic resonance imaging (MRI).
- The cornea is a component of the refractive system and measures 0.5 mm in thickness centrally. On MRI, the cornea is a low signal intensity convex structure due to the collagen content.
- The average depth of the normal anterior chamber is about 2.5 mm, but ranges from 1.5 to 4 mm depending on demographics (Fig. 2.9).
- The lens is an ovoid crystalline structure that forms the posterior boundary of the anterior chamber and is attached to the ciliary body via the zonular fibers. The lens displays low signal on both T1- and T2-weighted sequences and typically measures 5 mm in anteroposterior thickness and 9 mm in equatorial length (Fig. 2.10).

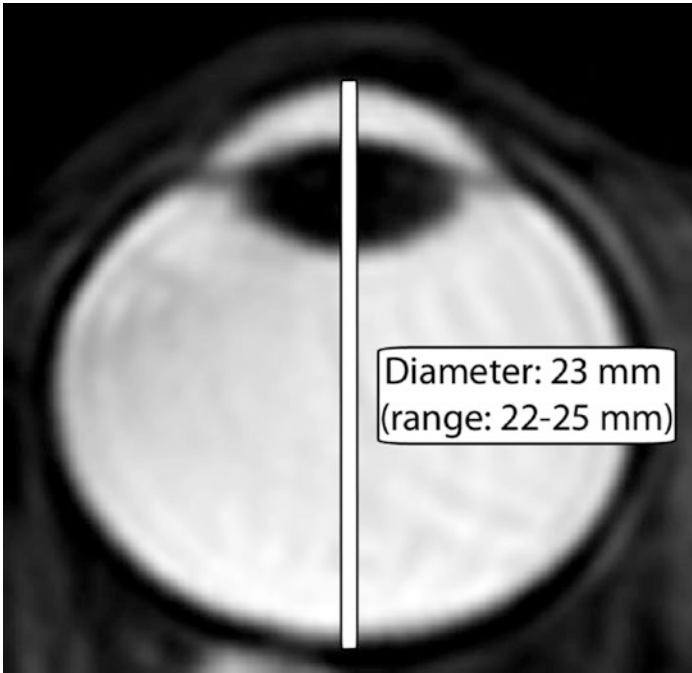


Fig. 2.8 Overall globe dimensions. Axial T2-weighted magnetic resonance imaging (MRI) shows the typical width and range of the adult globe diameter

- The vitreous humor comprises two-thirds of the volume of the globe.
- The posterior walls of the globes are typically 9–10 mm posterior to the interzygomatic line (Fig. 2.11).

Practical implications: The size of the globe is relevant for diagnosing buphthalmos or microphthalmos (Fig. 2.12). MRI ocular volumetry measurement error rates with RARE are lower than with FSPGR sequences. Fast spin echo (FSE) images acquired with fat suppression minimize chemical shift artifact in the region of the sclera. In any patient, a discrepancy on CT

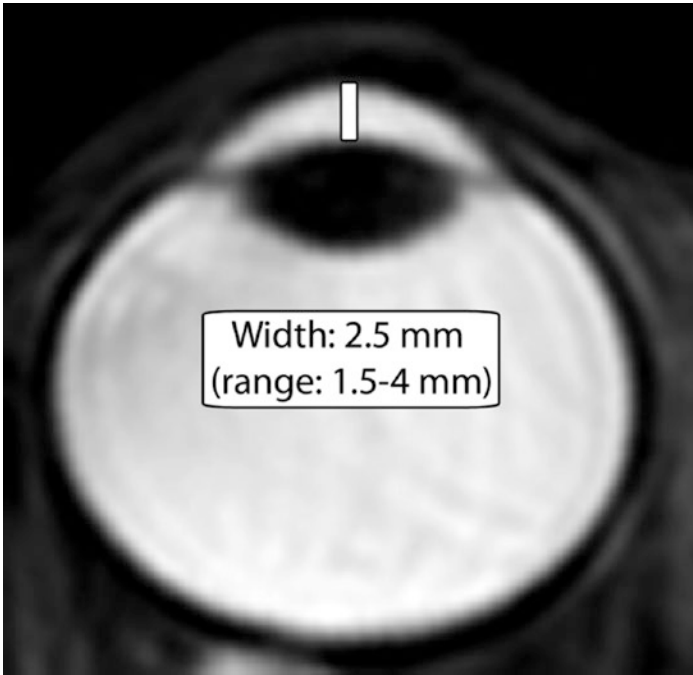


Fig. 2.9 Anterior chamber. Axial T2-weighted magnetic resonance imaging (MRI) shows the typical width and range of the normal adult anterior chamber

images of 2 mm or more between the depths of the anterior chambers of the normal and abnormal eyes or a depth measuring over 5 mm raises the possibility of scleral rupture (Fig. 2.13).

2.3 Optic Nerve and Sheath

The optic nerve is an extension of white matter tracts from the retina to the brain and is surrounded by cerebrospinal fluid that is continuous with the intracranial subarachnoid space. In turn, the

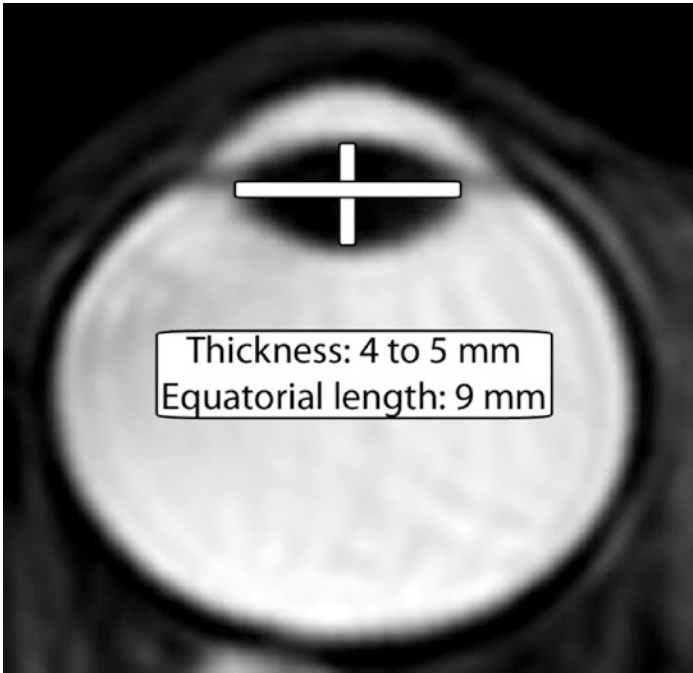


Fig. 2.10 Lens. Axial T2-weighted magnetic resonance imaging (MRI) shows the average dimensions of the adult lens

optic nerve sheath is a layer of dura that surrounds the optic nerve and cerebrospinal fluid. The optic nerve sheath can vary in width with changes in cerebrospinal fluid pressure.

- *Optic Nerve Width:*
 - Normal pediatric optic nerve diameters measured 10 mm posterior to the optic disk are listed in Table 2.1.
 - A lower bound to the 95% prediction interval for normal optic nerves is $(2.24 \text{ mm} + 0.05 \times [\text{age in years}]) \text{ mm}$.
 - Adult optic nerve diameter declines from the anterior to posterior orbit and measures 4.0 mm just posterior to the

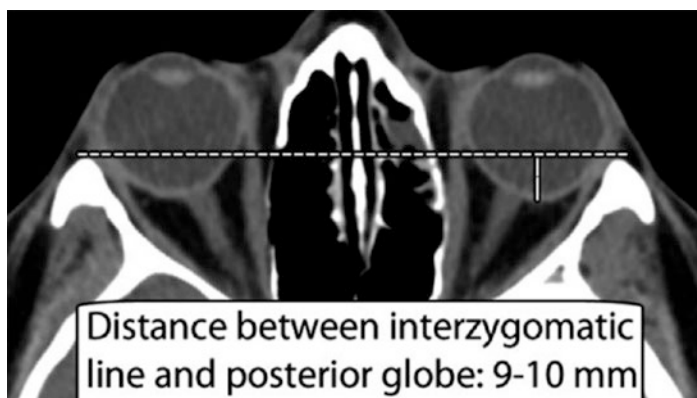


Fig. 2.11 Proptosis measurement. Axial computed tomography (CT) image denotes the typical normal position of the globe with respect to the interzygomatic line

globe and 3.5 mm at 10 mm posterior to the globe (Fig. 2.14).

- *Optic Nerve Length:*
 - Intraocular segment: 1 mm—emerges through the scleral opening
 - Intraorbital segment: 25 mm—the longest segment and the communication between subarachnoid space around the optic nerve with that in suprasellar cistern
 - Canalicular segment: 9 mm
- *Optic Nerve Sheath:*
 - Children, measured 10 mm anterior to the optic foramen on axial T2 sequence:
 - 0–3 years: 3.1 mm
 - 3–6 years: 4.1 mm
 - 6–18 years: 3.6 mm

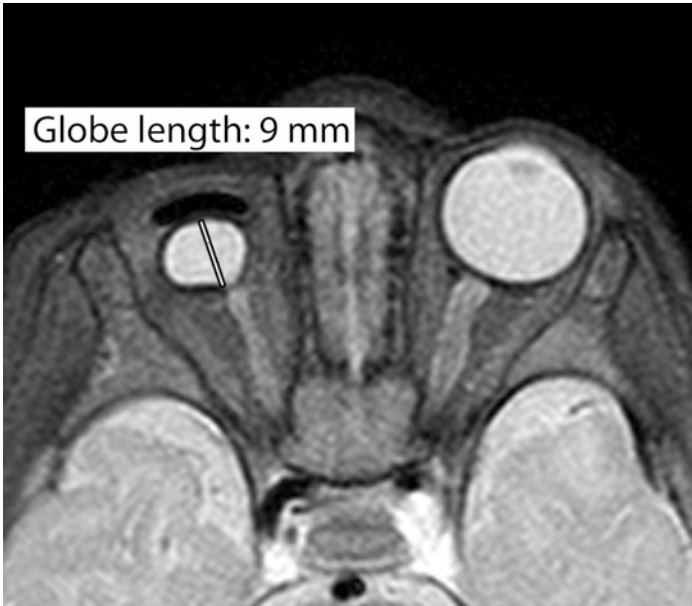


Fig. 2.12 Microphthalmos. Axial fat-suppressed T2-weighted magnetic resonance imaging (MRI) shows a small right globe

- Adults: The optic nerve sheath diameters on CT are $4.9\text{--}5.2 \pm 1.3\text{--}1.5$ mm at 3 mm, $4.4\text{--}4.5 \pm 0.6\text{--}0.8$ mm at 8 mm from the globe, and $3.6\text{--}3.7 \pm 0.7\text{--}0.8$ mm at 3 mm from the optic canal (Fig. 2.15).
- Normal values of the optic nerve sheath complex on CT (mean \pm 2 SDs) at the retrobulbar and waist regions are 5.6 ± 1.8 (3.8–7.4) mm and 3.7 ± 0.8 (2.9–4.5) mm, respectively.
- There is no correlation between age, gender, and size of the optic nerve sheath complex.

Practical implications: The least variable results are obtained 8–10 mm posterior to the globe. The optic nerve diameter is smaller in glaucoma patients but larger in patients with increased intracranial pressure. The anatomic extension of the subarachnoid



Fig. 2.13 Globe rupture. Axial computed tomography (CT) image shows collapse of the left anterior chamber (arrow) in a child who was stabbed in the eye with scissors

Table 2.1 Normal pediatric optic nerve diameters measured 10 mm posterior to the optic disk

Age (year)	Diameter (mm)
0–1.5	2.2
1.5–3	2.4
3–6	2.6
6–12	2.9
12–18	3.1

space underneath the optic nerve sheath is thought to be responsible for the transmission of these forces. Conditions in which the optic nerve sheath complex can be enlarged include neoplasms, such as gliomas (Fig. 2.16), pseudotumor, cerebri, infection, hemorrhage, and acute optic neuritis. The optic nerve sheath complex can be abnormally small in cases of chronic ischemia or septo-optic dysplasia.

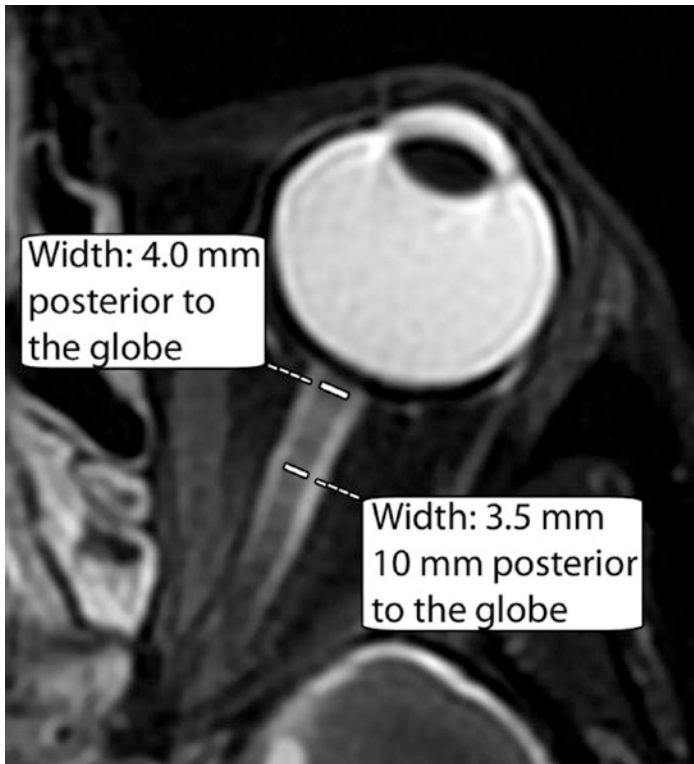


Fig. 2.14 Optic nerve. Axial T2-weighted magnetic resonance imaging (MRI) shows the typical widths of the optic nerve in an adult

2.4 Extraocular Muscles

- The extraocular muscles that are responsible for moving the globe include the superior, inferior, medial, and lateral recti and the superior and inferior oblique muscles.
- The levator palpebrae superioris is responsible for moving the superior eyelid.
- The normal sizes of the extraocular muscles in adults are listed in Table 2.2 and shown in Fig. 2.17.

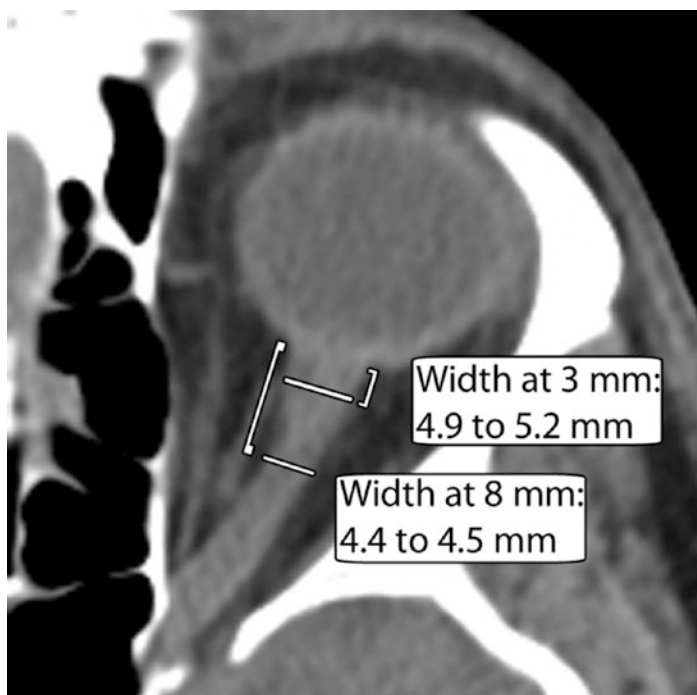


Fig. 2.15 Optic nerve sheath. Axial computed tomography (CT) image shows that the optic nerve sheath is typically wider just posterior to the globe versus more posteriorly

- All extraocular recti muscles increase in thickness from childhood, with the most dramatic growth occurring in the first 5–6 months of life. This growth continues as outlined in Table 2.2, until about 60 years old when the thickness begins to decline.
- The inferior rectus and superior group muscles are measured in the coronal plane, while the medial and lateral rectus muscles can be measured on the axial or coronal planes, but the coronal plane measurements tend to be 1.5 and 1.2 times

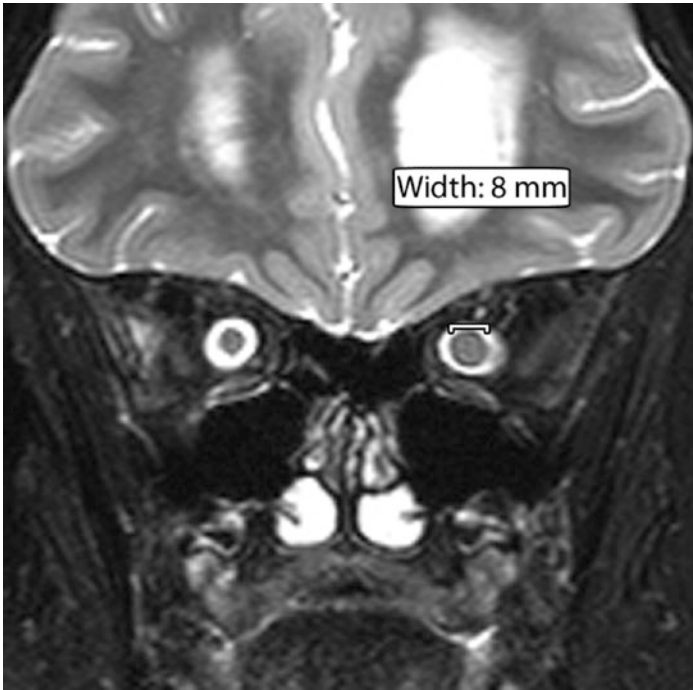


Fig. 2.16 Optic glioma. Coronal T2-weighted magnetic resonance imaging (MRI) shows enlargement of the left orbital optic nerve. There is also dilatation of the bilateral optic nerve sheaths and partly imaged dilatation of the left lateral ventricle in a patient with neurofibromatosis type 1

Table 2.2 Normal dimensions of the extraocular muscles in adults

Extraocular muscle	Maximum cross-sectional thickness (mm)	Maximum cross-sectional area (mm ²)
Medial rectus	3.5–4.2	27.9–30.3
Lateral rectus	3.2–3.3	32.2–41.2
Inferior rectus	4.2–4.8	28.0–33.6
Superior group ^a	3.9–4.6	33.0–34.4
Superior oblique	–	13.8–19.0
Inferior oblique	1.5–2.8	21.6

^aSince they cannot be reliably distinguished from each other, the superior rectus and the levator palpebrae superior muscles are measured together

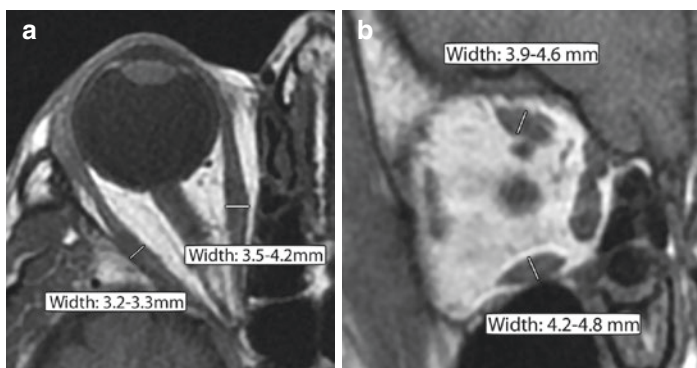


Fig. 2.17 Extraocular muscles. Axial (a) and coronal (b) T1-weighted MR images show the typical widths of the horizontal and vertical extraocular muscles

greater than the axial plane measurement for these muscles, respectively.

Practical implications: The mean diameters of the extraocular muscles in males are significantly larger than in females. Total extraocular muscle volume is not conserved, but actually increases with contraction and decreases with relaxation. Owing to the dramatic postnatal changes in extraocular muscle size and insertional position, it is generally safer to perform extraocular muscle surgery after about 6 months of age. Enlargement of the extraocular muscles, particularly the inferior, medial, and superior rectus muscles, can be a manifestation of thyroid eye disease (Fig. 2.18). Since denervated extraocular muscles do not readily atrophy, abnormally small muscles may be a sign of chronic progressive external ophthalmoplegia. Other conditions that can result in extraocular muscle enlargement include contusion, infection, and neoplasm.

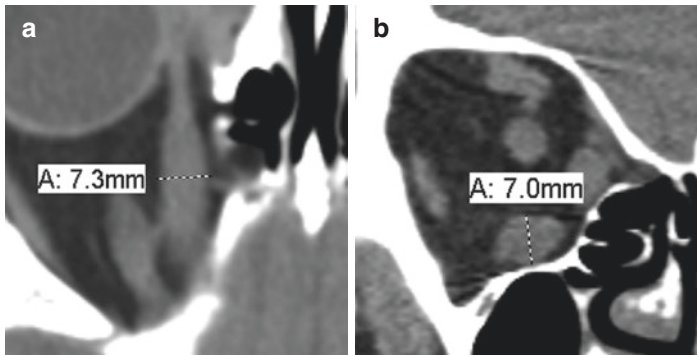


Fig. 2.18 Thyroid eye disease. Axial (a) and coronal (b) computed tomography (CT) images show enlargement of multiple right inferior and medial rectus muscles

2.5 Lacrimal Gland

- The lacrimal gland produces the aqueous portion of the tear film and is located in the anterior, superotemporal orbit within the lacrimal fossa of the frontal bone.
- Secretions are emptied into a duct system that delivers the fluid to the ocular surface. The outflow component of the lacrimal system lies at the nasal side of the eye, where puncta located on the upper and lower lids drain fluid into canaliculi that lead to the nasolacrimal sac and nasal cavity.
- The lacrimal gland can have a bilobed shape due to indentation by the levator palpebrae superioris tendon, with a small palpebral component underneath the eyelid and a larger orbital component.
- The average dimensions of the lacrimal gland are as follows (Fig. 2.19):
 - Axial width: 5 mm
 - Axial length: 15 mm
 - Coronal height: 20 mm

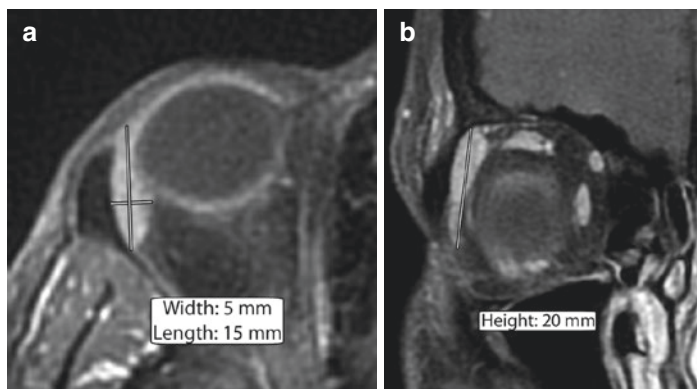


Fig. 2.19 Lacrimal gland. Axial (a) and coronal (b) post-contrast T1-weighted MR images show the typical dimensions of the normal lacrimal gland

- The mean volume for lacrimal glands in adults ranges from 0.7 to 0.8 cm³.

Practical implications: Lacrimal gland volume and dimensions decrease with age, but there is no significant variation with gender or laterality. Lacrimal gland measurements may differ between ethnicities. Lacrimal glands in the patients with Sjögren syndrome can be hypertrophic, normal in size, or atrophic. Accelerated fat deposition can be detected with MR imaging and can be a distinctive feature of lacrimal glands that are affected by Sjögren's syndrome. A significant increase in lacrimal gland volume can be seen in thyroid-associated ophthalmopathy patients. The lacrimal gland can also be diffusely enlarged in other conditions, including sarcoidosis, orbital inflammation, and neoplasms, such as lymphoma (Fig. 2.20).



Fig. 2.20 Lacrimal gland lymphoma. Axial post-contrast T1-weighted magnetic resonance imaging (MRI) shows asymmetric diffuse enlargement of the right lacrimal gland

2.6 Superior Ophthalmic Vein

- The superior ophthalmic vein typically originates from the junction of the supraorbital and angular veins, approximately 4–5 mm posterior to the superior oblique tendon.
- The superior ophthalmic vein joins the inferior ophthalmic vein and passes through the superior orbital fissure.
- The superior ophthalmic vein consistently runs lateral to the ophthalmic artery, but has an asymmetric outer diameter bilaterally. The mean outer diameter at the crossing point is 1.6–1.7 mm (Fig. 2.21).

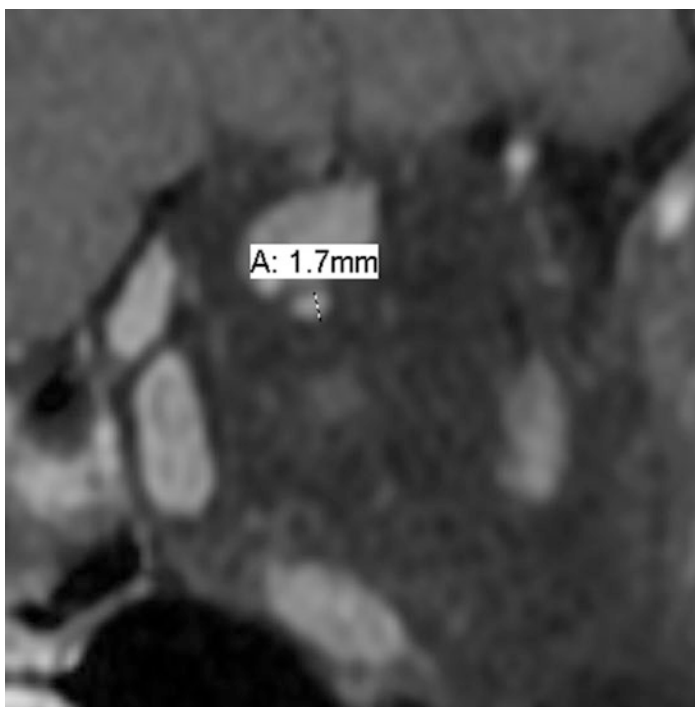


Fig. 2.21 Superior ophthalmic vein. Coronal post-contrast fat-suppressed T1-weighted magnetic resonance imaging (MRI) shows the typical dimension of the vessel

Practical implications: Enlargement of the superior ophthalmic vein can be associated with carotid-cavernous fistulas, arteriovenous malformations, thrombosis, compression, thyroid eye disease, orbital pseudotumors, retrocavernous tumors, elevated intracranial pressure, and intubation (Fig. 2.22). A diameter of ≥ 2 mm on axial CT scans is a possible indicator of enlargement, diameter ≥ 3 mm is likely to be an indicator, and diameter ≥ 4 mm is a definite indicator.

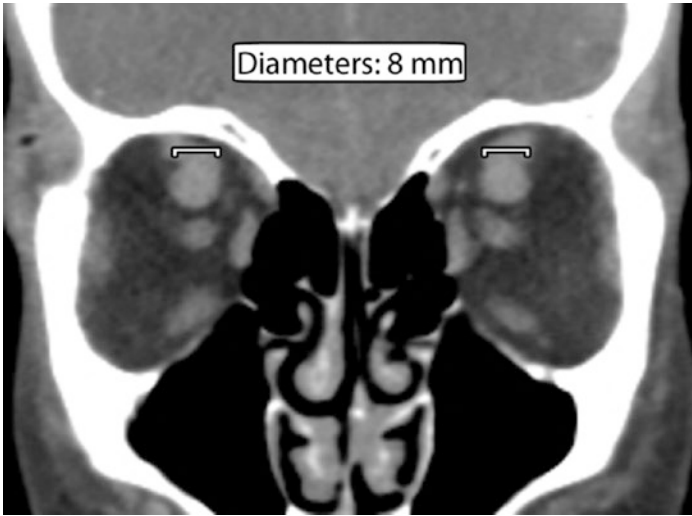


Fig. 2.22 Superior ophthalmic vein enlargement. Coronal computed tomography (CT) image shows the superior ophthalmic veins are significantly enlarged bilaterally in a patient with congestive heart failure and intubation

Further Reading

- Ankur G, Xin Z. Lacrimal gland development: from signaling interactions to regenerative medicine. *Dev Dyn.* 2017;246(12):970–80.
- Bingham CM, Castro A, Realini T, Nguyen J, Hogg JP, Sivak-Callcott JA. Calculated CT volumes of lacrimal glands in normal Caucasian orbits. *Ophthalmic Plast Reconstr Surg.* 2013;29(3):157–9.
- Bourlet P, Carrie D, Garcier JM, Dalens H, Chansolme D, Viallet JF, Boyer L. Study of the inferior oblique muscle of the eye by MRI. *Surg Radiol Anat.* 1998;20(2):119–21.
- Bukhari AA, Basheer NA, Joharjy HI. Age, gender, and interracial variability of normal lacrimal gland volume using MRI. *Ophthalmic Plast Reconstr Surg.* 2014;30(5):388–91.
- Carlow TJ, Depper MH, Orrison WW Jr. MR of extraocular muscles in chronic progressive external ophthalmoplegia. *AJNR Am J Neuroradiol.* 1998;19(1):95–9.
- Clark RA, Demer JL. Changes in extraocular muscle volume during ocular duction. *Invest Ophthalmol Vis Sci.* 2016;57(3):1106–11.

- De Battista JC, Zimmer LA, Theodosopoulos PV, Froelich SC, Keller JT. Anatomy of the inferior orbital fissure: implications for endoscopic cranial base surgery. *J Neurol Surg B Skull Base*. 2012;73(2):132–8.
- Elhadi AM, Zaidi HA, Yagmurlu K, Ahmed S, Rhoton AL Jr, Nakaji P, Preul MC, Little AS. Infraorbital nerve: a surgically relevant landmark for the pterygopalatine fossa, cavernous sinus, and anterolateral skull base in endoscopic transmaxillary approaches. *J Neurosurg*. 2016;125(6):1460–8.
- Erdogan B, Alper Y, Bahar Y, Hasmet Y, Gulen D. Evaluation of lacrimal gland dimensions and volume in Turkish population with computed tomography. *J Clin Diagn Res*. 2016;10(2):TC06–8.
- Hallinan JT, Pillay P, Koh LH, Goh KY, Yu WY. Eye globe abnormalities on MR and CT in adults: an anatomical approach. *Korean J Radiol*. 2016;17(5):664–73.
- Hashemi H, Khabazkhoob M, Miraftab M, Emamian MH, Shariati M, Abdolahinia T, Fotouhi A. The distribution of axial length, anterior chamber depth, lens thickness, and vitreous chamber depth in an adult population of Shahroud, Iran. *BMC Ophthalmol*. 2012;12:50.
- Hashemi H, Jafarzadehpur E, Ghaderi S, Yekta A, Ostadimoghaddam H, Norouzirad R, Khabazkhoob M. Ocular components during the ages of ocular development. *Acta Ophthalmol*. 2015;93(1):e74–81.
- Huanmanop T, Agthong S, Chentanez V. Surgical anatomy of fissures and foramina in the orbits of Thai adults. *J Med Assoc Thai*. 2007;90(11):2383–91.
- Hyoun-Do H, Ji-Hye K, Seong-Jae K, Ji-Myong Y, Seong-Wook S. The change of lacrimal gland volume in Korean patients with thyroid-associated ophthalmopathy. *Korean J Ophthalmol*. 2016;30(5):319–25.
- Izumi M, Eguchi K, Uetani M, Nakamura H, Takagi Y, Hayashi K, et al. MR features of the lacrimal gland in Sjögren's syndrome. *Am J Roentgenol*. 1998;170:1661–6.
- Karakaş P, Bozkir MG, Oguz O. Morphometric measurements from various reference points in the orbit of male Caucasians. *Surg Radiol Anat*. 2003;24(6):358–62.
- Karim S, Clark RA, Poukens V, Demer JL. Demonstration of systematic variation in human intraorbital optic nerve size by quantitative magnetic resonance imaging and histology. *Invest Ophthalmol Vis Sci*. 2004;45(4):1047–51.
- Kashiwagi K, Okubo T, Tsukahara S. Association of magnetic resonance imaging of anterior optic pathway with glaucomatous visual field damage and optic disc cupping. *J Glaucoma*. 2004;13(3):189–95.
- Laestadius ND, Aase JM, Smith DW. Normal inner canthal and outer orbital dimensions. *J Pediatr*. 1969;74(3):465–8.
- Lee JS, Lim DW, Lee SH, Oum BS, Kim HJ, Lee HJ. Normative measurements of Korean orbital structures revealed by computerized tomography. *Acta Ophthalmol Scand*. 2001;79(2):197–200.

- Lee H, Lee Y, Ha S, Park M, Baek S. Measurement of width and distance of the posterior border of the deep lateral orbital wall using computed tomography. *J Craniomaxillofac Surg.* 2011;39(8):606–9.
- Lee JS, Lee H, Kim JW, Chang M, Park M, Baek S. Computed tomographic dimensions of the lacrimal gland in healthy orbits. *J Craniofac Surg.* 2013;24(3):712–5.
- Lefebvre DR, Yoon MK. CT-based measurements of the sphenoid trigone in different sex and race. *Ophthalmic Plast Reconstr Surg.* 2015;31(2):155–8.
- Lenhart PD, Desai NK, Bruce BB, Hutchinson AK, Lambert SR. The role of magnetic resonance imaging in diagnosing optic nerve hypoplasia. *Am J Ophthalmol.* 2014;158(6):1164–1171.e2.
- Lerdlum S, Boonsirikamchai P, Setsakol E. Normal measurements of extraocular muscle using computed tomography. *J Med Assoc Thai.* 2007;90(2):307–12.
- Lirng JF, Fuh JL, Wu ZA, Lu SR, Wang SJ. Diameter of the superior ophthalmic vein in relation to intracranial pressure. *AJNR Am J Neuroradiol.* 2003;24(4):700–3.
- Mafee MF, Pruzansky S, Corrales MM, Phatak MG, Valvassori GE, Dobben GD, Capek V. CT in the evaluation of the orbit and the bony interorbital distance. *AJNR Am J Neuroradiol.* 1986;7(2):265–9.
- Maresky HS, Ben Ely A, Bartischovsky T, Coret-Simon J, Morad Y, Rozowsky S, Klar M, Negieva S, Bekerman I, Tal S. MRI measurements of the normal pediatric optic nerve pathway. *J Clin Neurosci.* 2018;48:209–13.
- Nam Y, Bahk S, Eo S. Anatomical study of the infraorbital nerve and surrounding structures for the surgery of orbital floor fractures. *J Craniofac Surg.* 2017;28(4):1099–104.
- Nguyen DC, Farber SJ, Um GT, Skolnick GB, Woo AS, Patel KB. Anatomical study of the intraosseous pathway of the infraorbital nerve. *J Craniofac Surg.* 2016;27(4):1094–7.
- Nugent RA, Belkin RI, Neigel JM, Rootman J, Robertson WD, Spinelli J, Graeb DA. Graves orbitopathy: correlation of CT and clinical findings. *Radiology.* 1990;177(3):675–82.
- Ozgen A, Ariyurek M. Normative measurements of orbital structures using CT. *AJR Am J Roentgenol.* 1998;170(4):1093–6.
- Ozgen A, Aydingöz U. Normative measurements of orbital structures using MRI. *J Comput Assist Tomogr.* 2000;24(3):493–6.
- Pool GM, Didier RA, Bardo D, Selden NR, Kuang AA. Computed tomography-generated anthropometric measurements of orbital relationships in normal infants and children. *J Neurosurg Pediatr.* 2016;18(2):201–6.
- Saccà S, Polizzi A, Macrì A, Patrone G, Rolando M. Echographic study of extraocular muscle thickness in children and adults. *Eye (Lond).* 2000;14(5):765–9.
- Shofty B, Ben-Sira L, Constantini S, Freedman S, Kesler A. Optic nerve sheath diameter on MR imaging: establishment of norms and comparison

- of pediatric patients with idiopathic intracranial hypertension with healthy controls. *AJNR Am J Neuroradiol.* 2012;33(2):366–9.
- Suh JD, Kuan EC, Thompson CF, Scawn RL, Feinstein AJ, Barham HP, Kingdom TT, Ramakrishnan VR. Using fixed anatomical landmarks to avoid medial rectus injury: a radiographic analysis in patients with and without Graves' disease. *Am J Otolaryngol.* 2016;37(4):334–8.
- Swan KC, Wilkins JH. Extraocular muscle surgery in early infancy—anatomical factors. *J Pediatr Ophthalmol Strabismus.* 1984;21(2):44–9.
- Tanitime K, Sone T, Miyoshi T, Tanitime N, Otani K, Akiyama Y, Takasu M, Date S, Kiuchi Y, Awai K. Ocular volumetry using fast high-resolution MRI during visual fixation. *AJNR Am J Neuroradiol.* 2013;34(4):870–6.
- Tian S, Nishida Y, Isberg B, Lennerstrand G. MRI measurements of normal extraocular muscles and other orbital structures. *Graefes Arch Clin Exp Ophthalmol.* 2000;238(5):393–404.
- Tsutsumi S, Nakamura M, Tabuchi T, Yasumoto Y. The superior ophthalmic vein: delineation with high-resolution magnetic resonance imaging. *Surg Radiol Anat.* 2015;37(1):75–80.
- Turvey TA, Golden BA. Orbital anatomy for the surgeon. *Oral Maxillofac Surg Clin North Am.* 2012;24(4):525–36.
- Vaiman M, Abuita R, Bekerman I. Optic nerve sheath diameters in healthy adults measured by computer tomography. *Int J Ophthalmol.* 2015;8(6):1240–4.
- Watcharakorn A, Ngamsirisuk S. Normal measurements of size of optic nerve sheath complex using computed tomography. *J Med Assoc Thai.* 2014;97(Suppl 8):S22–6.
- Weissman JL, Beatty RL, Hirsch WL, Curtin HD. Enlarged anterior chamber: CT finding of a ruptured globe. *AJNR Am J Neuroradiol.* 1995;16(4 Suppl):936–8.